Relationship between Solution Structure and Phase Behavior: A Neutron Scattering Study of Concentrated Aqueous Hexamethylenetetramine Solutions

R. C. Burton,[†] E. S. Ferrari,[†] R. J. Davey,*[,†] J. L. Finney,[‡] and D. T. Bowron[§]

Molecular Materials Centre, School of Chemical Engineering & Analytical Science, The University of Manchester, P.O. Box 88, Manchester M60 1QD, U.K., Department of Physics & Astronomy, University College London, Gower Street, London WC1E 6BT, U.K., and ISIS Facility, CLRC Rutherford Appleton Laboratory, Chilton, Didcot, Oxon, OX11 0QX, U.K.

Received: December 31, 2008; Revised Manuscript Received: February 26, 2009

The water−hexamethylenetetramine system displays features of significant interest in the context of phase equilibria in molecular materials. First, it is possible to crystallize two solid phases depending on temperature, both hexahydrate and anhydrous forms. Second, saturated aqueous solutions in equilibrium with these forms exhibit a negative dependence of solubility (retrograde) on temperature. In this contribution, neutron scattering experiments (with isotopic substitution) of concentrated aqueous hexamethylenetetramine solutions combined with empirical potential structure refinement (EPSR) were used to investigate the time-averaged atomistic details of this system. Through the derivation of radial distribution functions, quantitative details emerge of the solution coordination, its relationship to the nature of the solid phases, and of the underlying cause of the solubility behavior of this molecule.

Background

Our fundamental understanding of the relationship between liquid phase structure and the nature of binary and ternary phase behavior underlies many important physical processes including distillation in vapor−liquid systems, extraction in liquid−liquid systems, and crystallization and solubility in solid−liquid systems. Deviations of thermodynamic properties from the ideal state are conventionally quantified in terms of activity coefficients[1] with direct studies of intermolecular interactions increasingly possible in concentrated systems as a result of recent developments in spectroscopic and scattering techniques.[2−4] Of particular interest in the current work is the combined application of neutron scattering data (obtained with isotopic substitution) and empirical potential structure refinement (EPSR)[5,6] for the determination of the structure of a two-component solution. EPSR, an iterative procedure based on a Monte Carlo computer simulation, is used to give a model structure consistent with measured scattering data. Such studies have successfully yielded information for liquid−liquid systems such as methanol−water[7] and tertiary butanol−water mixtures[8] as well as dilute and concentrated aqueous urea solutions.[9,10]

In the current work we have turned our attention to the cage-like molecule, hexamethylenetetramine (HMT, hexamine, urotropine). Its molecular structure and molecular center used in the current data analysis are shown in Figures 1a and 1b. The binary phase diagram of HMT in water is seen in Figure 1c, taken from White.[11] It exhibits two known solid phases: an anhydrous phase (HXMTAM07[12,13]), and a hexahydrate, $C_6H_{12}N_4.6H_2O$ (HXMTHH[14]) which is stable below 13.5 °C.[11,15] The anhydrous phase is highly soluble in water, having an unusual *negative* temperature solubility coefficient[11] with a solubility minimum at around 75−80 °C. The origin of this retrograde solubility and its links to the binary phase diagram are the subject of this current study.

Anhydrous HMT crystallizes as colorless rhombic dodecahedral crystals belonging to the cubic system, space group $I\bar{4}3m$[12,16,17] while the hexahydrate is a clathrate-type crystal structure, space group *R*3*m*, in which HMT sits in cavities within a hydrogen bonded network of water molecules.[14,18] Figure 1d shows a view of the anhydrous body centered lattice of the crystalline anhydrate, highlighting the three weak N···H−C intermolecular interactions at 2.89 Å. These correspond to the packing of molecules shown by Figure 1e in which the face of one molecule accepts a neighbor. Figure 1f shows a view of the hydrated environment of HMT within the hexahydrate from which it is evident that three of the nitrogen atoms are hydrogen bonded to water with three other water molecules interacting through weaker C−H···O contacts.

Activity coefficients measured previously for aqueous HMT at 25 °C by Crescenzi et al.[19] and Quadrifoglio et al.[20] for saturated solutions at 25 °C, 30 °C, and 35 °C show very strong deviations from ideal solution behavior which have been interpreted in terms of a 'structuring' of water[19] consistent with restriction of water molecules in a solvation cage around the HMT.

This has led to the idea that HMT promotes some kind of enhanced water structure through hydrogen bonds between the HMT nitrogen atoms and water above 0 °C since this type of interaction also occurs in the hydrate. A corollary of this idea (Barone et al.[21]) is that as the hydrogen bonded structure of water breaks down with increasing temperature, HMT would be less likely to be accommodated, and hence the solubility of aqueous HMT decreases with increasing temperature.

Overall this unusual solution chemistry together with the existence of both anhydrous and hydrated solid phases suggested aqueous HMT as an important system for study, and we have therefore explored its solution chemistry in atomic detail through the atom−atom radial distribution functions provided by combined neutron scattering and EPSR.

* To whom correspondence should be addressed.
[†] The University of Manchester.
[‡] University College London.
[§] CLRC Rutherford Appleton Laboratory.

10.1021/jp811515u CCC: $40.75
Published on Web 04/07/2009

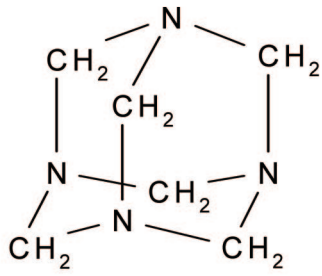

(a)

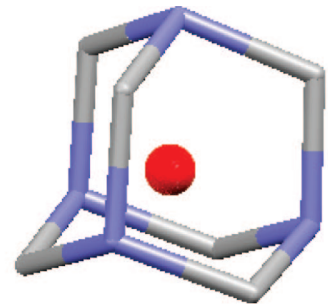

(b)

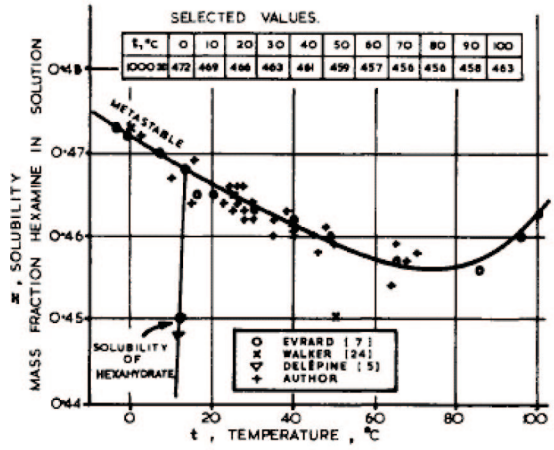

(c)

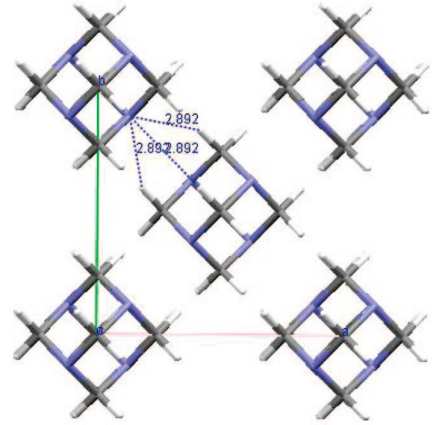

(d)

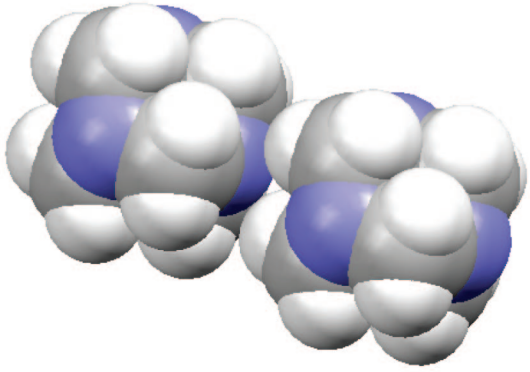

(e)

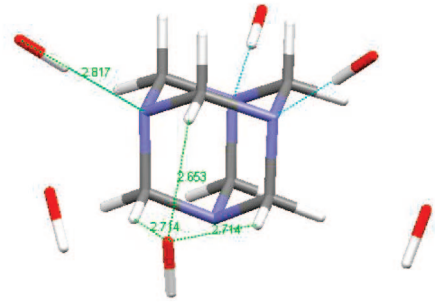

(f)

Figure 1. (a) The molecular structure of HMT, (b) the HMT molecule (red sphere is the molecular center) used to generate the molecular centers' functions (taken from HMTAM07[13,14]), (c) the binary HMT−water phase diagram reproduced from ref 11, (d) crystal packing of HMT, (e) intermolecular face to face contact between HMT molecules in the crystal, (f) the water−HMT interactions in the hexahydrate.[15] (white hydrogen, gray carbon, blue nitrogen, red oxygen; in f, only one hydrogen per water is shown).

Experimental Section

To perform scattering experiments giving appropriate contrast to interactions of interest, it is necessary to use isotopically substituted samples.[22] Hence, the hydrogenated and deuterated ($C_6H_{12}N_4$ and $C_6D_{12}N_4$) forms of HMT, together with H_2O and D_2O, were used to prepare the following solutions in order to extract structural data for the aqueous HMT from the neutron scattering measurements: for HMT−HMT correlations, $(CH_2)_6N_4$ in D_2O, $(CD_2)_6N_4$ in D_2O, and a 1:1 mixture of $(CH_2)_6N_4$:$(CD_2)_6N_4$ in D_2O; for the water−water correlations, $(CD_2)_6N_4$ in H_2O, $(CD_2)_6N_4$ in D_2O, and $(CD_2)_6N_4$ in a 1:1 mixture of H_2O:D_2O; for the water−HMT correlations, $(CH_2)_6N_4$ in H_2O, $(CD_2)_6N_4$ in D_2O and a 1:1 mixture of $(CH_2)_6N_4$:$(CD_2)_6N_4$ in 1:1 mixture of H_2O:D_2O. These experiments required seven isotopically distinct samples for each concentration studied and were chosen to provide a tight constraint on the molecular configurations of the solution structure generated by the EPSR model. All chemicals were purchased from Cambridge Isotope Laboratories.

Since it was initially our intention to study both saturated and supersaturated solutions, the solubilities of HMT in water, HMT in D_2O, and D-HMT in H_2O were measured gravimetrically and compared to previous data.[11] It was found that for HMT in D_2O the measured solubilities at 10, 25, and 80 °C (±0.1 °C) were respectively 0.0964, 0.952, and 0.0919 mol

fraction, 5− 10% lower than values for HMT and D-HMT in H_2O which were consistent with White's data (ref 11, Figure 1c above). This difference precluded data collection in supersaturated or saturated solutions. Instead it was decided to work at 25 °C in both the dilute 0.050 mol fraction and the more concentrated 0.095 mol fraction solutions and at 80 °C in only the more concentrated 0.095 mol fraction solution. At 25 and 80 °C the saturation compositions for the hydrogenated system are 0.1002 and 0.0960 mol fraction of HMT, respectively, so that this higher concentration represents a slightly undersaturated solution at both temperatures. It was hoped that these experiments would not only show the concentration dependence of the structure but also give clues to the underlying causes for the retrograde solubility and the appearance of both hydrated and anhydrous crystalline phases.

The density of aqueous HMT solutions having the compositions used in the experiments were measured (Anton Paar Density Meter) to be 1.064×10^3 kgm^{-3} at 0.050 mol fraction and 25 °C and for 0.095 mol fraction, 1.106×10^3 and 1.072×10^3 kgm^{-3} at 25 and 80 °C, respectively.

The neutron scattering experiments were performed using the Small Angle Neutron Diffractometer for Amorphous and Liquid Samples (SANDALS) at the ISIS pulsed neutron source at the Rutherford Appleton Laboratory, UK. Data were collected from samples contained in a titanium−zirconium alloy sample cell in periods of 6 h per sample. This type of cell gives a negligible coherent scattering contribution to the measured signal and has internal dimensions of 1 mm × 35 mm × 35 mm so that approximately 1.5 mL of solution was used in each cell. The cell was mounted in a holder, the temperature of which was controlled to a stability of ±0.1 °C using a circulating water bath.

The data acquired from the solutions allowed the total interference differential cross-sections, $F(Q)$, (in which Q is the scattering vector, $Q = (4\pi)/(\lambda)\sin\theta$) to be generated, from which a structural model was produced using EPSR. The data were collected over scattering angles (2θ) between 3° and 40° and analyzed using the Gudrun routines[23] for neutron wavelengths in the range, $\lambda = 0.05-4.95$ Å.

Data Analysis

Empirical potential structure refinement[24,5,6] has been used to build atomistic structural models of the 0.050 and 0.095 mol fraction aqueous solutions of HMT at the investigated temperatures of 25 and 80 °C. This method generates three-dimensional structures that are consistent with the measured neutron scattering data obtained from solutions studied. The technique starts with a standard Monte Carlo simulation of a liquid that is first allowed to equilibrate under a reference set of atomic interaction potentials.[9] These are defined by Lennard−Jones parameters and coulomb charges. Once the simulation has reached equilibrium with the reference potentials, a difference function is calculated between the neutron scattering structure factors calculated from the model and those measured in the experiment. This difference function is used to derive a series of perturbation potentials that are combined with the reference functions.[24] The Monte Carlo algorithm is then continued under the new set of interaction potentials, and periodically the perturbation functions are re-evaluated. Ultimately this procedure generates a set of perturbation potentials that combine with the initial reference set to produce structural configurations within the simulation that agree with the experimental data used to drive the refinement. Once this hybrid set of potentials has been derived, the Monte Carlo simulation is continued and ensemble average information is accumulated on the structural configurations of the atoms and molecules in the standard way. The combination of geometrical and density constraints imposed by the simulation restrict the range of the experimental results to a physically and chemically consistent set of structural solutions. This is the primary advantage of the EPSR method for the interpretation of experimental scattering data over more conventional direct analysis approaches.

TABLE 1: HMT Bond Lengths and Angles Used during the EPSR Simulations to Constrain the Molecular Geometry[27,28]

bond lengths, Å		bond angles, deg	
C−N	1.448	N−C−N	111.2
C−H	1.090	N−C−H	109.5
		H−C−H	107.8
		C−N−C	109.5

TABLE 2: Bond Lengths and Angles for Water Used in the Simulations[9]

OW−HW: bond length, Å	HW−OW−HW: bond angle, deg
0.9076	104.5

TABLE 3: Lennard−Jones Parameters and Charges Used for the Atoms in HMT[27]

atom	Lennard−Jones well depth, kJ mol^{-1}	core diameter, Å	Coulomb charge
C	0.25104	3.5	0.18
N	0.71128	3.3	−0.54
H	0.06276	2.5	0.09

Within these simulations the average molecular geometry of the mixture constituents were constrained to the bond lengths and angles of Table 1 for HMT and Table 2 for water. The SPC/E model of Berendsen et al.[25] was used to describe water, and to account for the intrinsic molecular structural disorder that is captured by the structural measurements, the instantaneous molecular geometries of the mixture components were periodically randomized within a simple harmonic potential model that aimed to capture the unavoidable quantum mechanical zero point disorder.[26]

For HMT the Lennard−Jones parameters and effective charges used in EPSR were taken from ref 27 and are shown in Table 3. From Figure 1a and 1b it can be seen that the individual carbon, nitrogen, and hydrogen sites in HMT are all indistinguishable.

For 0.095 mol fraction aqueous HMT, EPSR was used on a box of 57 HMT and 543 water molecules. At 25 °C the box had a side length of 29.9 Å and atomic density of 0.108 atoms Å^{-3}. For 80 °C the box had a side length of 30.2 Å and atomic density of 0.105 atoms Å^{-3}. At both temperatures the empirical potential evolved over 10 000 Monte Carlo cycles, and finally ensemble accumulations were undertaken for 20 000 cycles. In each Monte Carlo cycle every atom, molecule, and rotational group in the simulation is moved once. To compare coordination numbers for the 0.095 mol fraction solution at 25 and 80 °C, the same atomic density was used at each temperature since it differs by less than 5%.

For the 0.050 mol fraction at 25 °C, EPSR was used on a box of 30 HMT and 570 water molecules with a side length of 30.2 Å and atomic density of 0.105 atoms Å^{-3}. Following equilibration the empirical potential evolved for 10 000 cycles and ensemble accumulations were then collected for a further 50 000 cycles. This higher number of accumulation cycles compared to the 0.095 concentration was necessary because of the lower concentration of HMT.

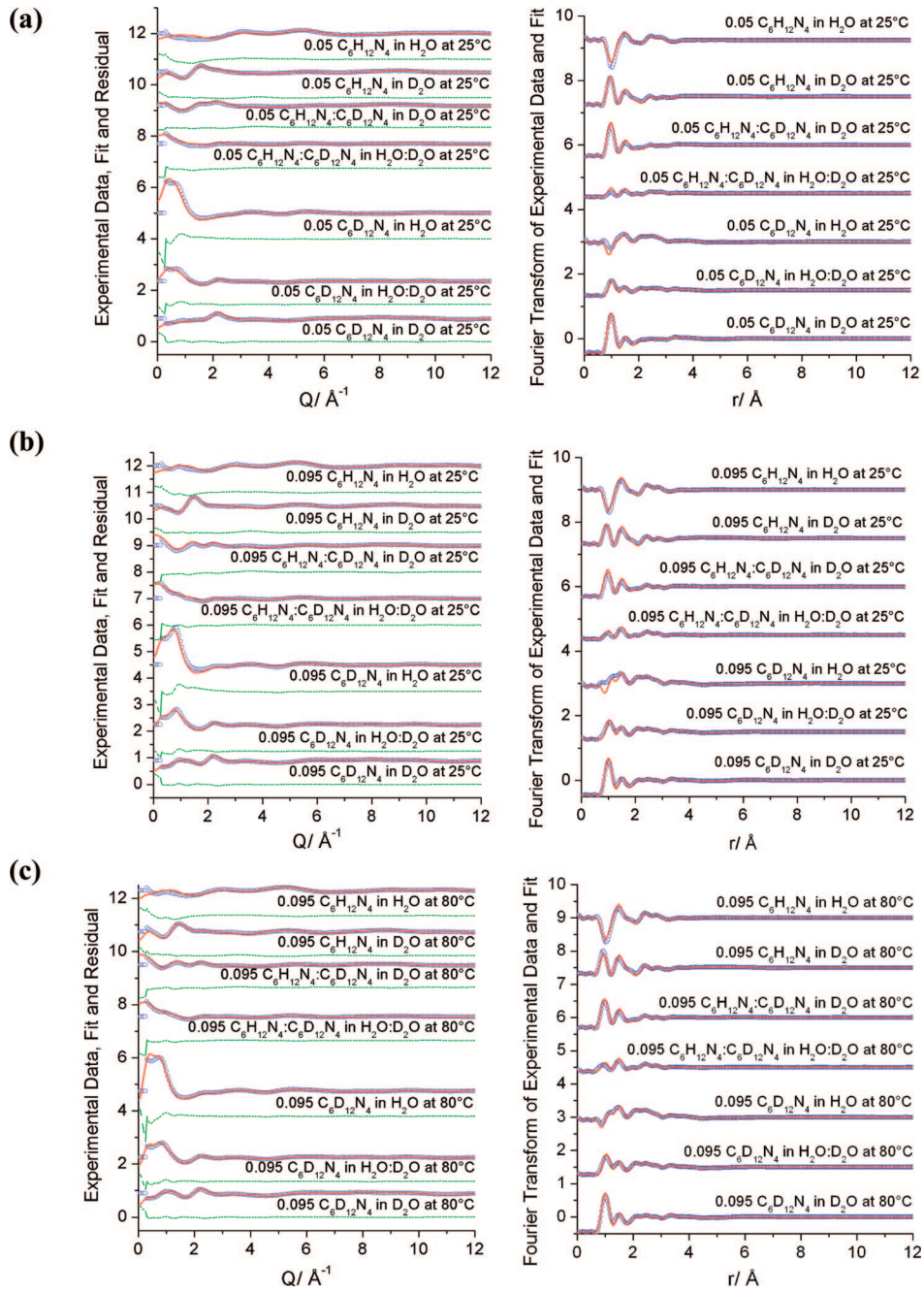

Figure 2. (Left) Experimentally measured $F(Q)$s (blue circles), EPSR fits (red solid lines), and residuals (dotted green lines) and (Right) composite $g(r)$s determined by Fourier transform of the experimental $F(Q)$s (blue circles) and EPSR fits (solid red lines). Graphs have been offset for clarity. From top to bottom are shown either $F(Q)$ (left column) or $g(r)$ (right column) for $C_6H_{12}N_4$ in H_2O, $C_6H_{12}N_4$ in D_2O, $C_6H_{12}N_4$:$C_6D_{12}N_4$ in D_2O, $C_6H_{12}N_4$:$C_6D_{12}N_4$ in H_2O:D_2O, $C_6D_{12}N_4$ in H_2O, $C_6D_{12}N_4$ in H_2O:D_2O, and finally $C_6D_{12}N_4$ in D_2O (a) 0.05 mol fraction of aqueous HMT at 25 °C, (b) 0.095 mol fraction of aqueous HMT at 25 °C, (c) 0.095 mol fraction of aqueous HMT at 80 °C.

Results and Discussion

The seven interference differential cross-sections generated from the isotopically distinct measurements at the two different temperatures and compositions can be seen in Figure 2 along with the neutron diffraction data and the EPSR fit residuals. It is clear that the fit to the data is good for all of the different neutron diffraction data sets. In some cases (e.g., Figure 2b, Fourier transform of $C_6D_{12}N_4/H_2O$) there are deviations between the measured data and the EPSR fit below $Q < 2.5$ Å. These discrepancies are due to inelastic and self-scattering, and although the data is corrected for these effects empirically, it is hard to avoid small residual systematic errors in the low Q region. It has been shown elsewhere[29] that these deviations give rise to a systematic error in real space that occurs at distances smaller that the first interatomic distances in the radial distribution functions and hence do not make any difference to the correlations at the relevant intermolecular length scales.[30,31] The magnitude of these effects is greater for the nondeuterated solutions, as the mass of the hydrogen atoms is closely comparable to the mass of the neutron, and consequently the corrections required to extract the differential scattering cross-sections from the raw experimental data are larger and more poorly defined. For this reason the EPSR technique has been used to analyze the data,

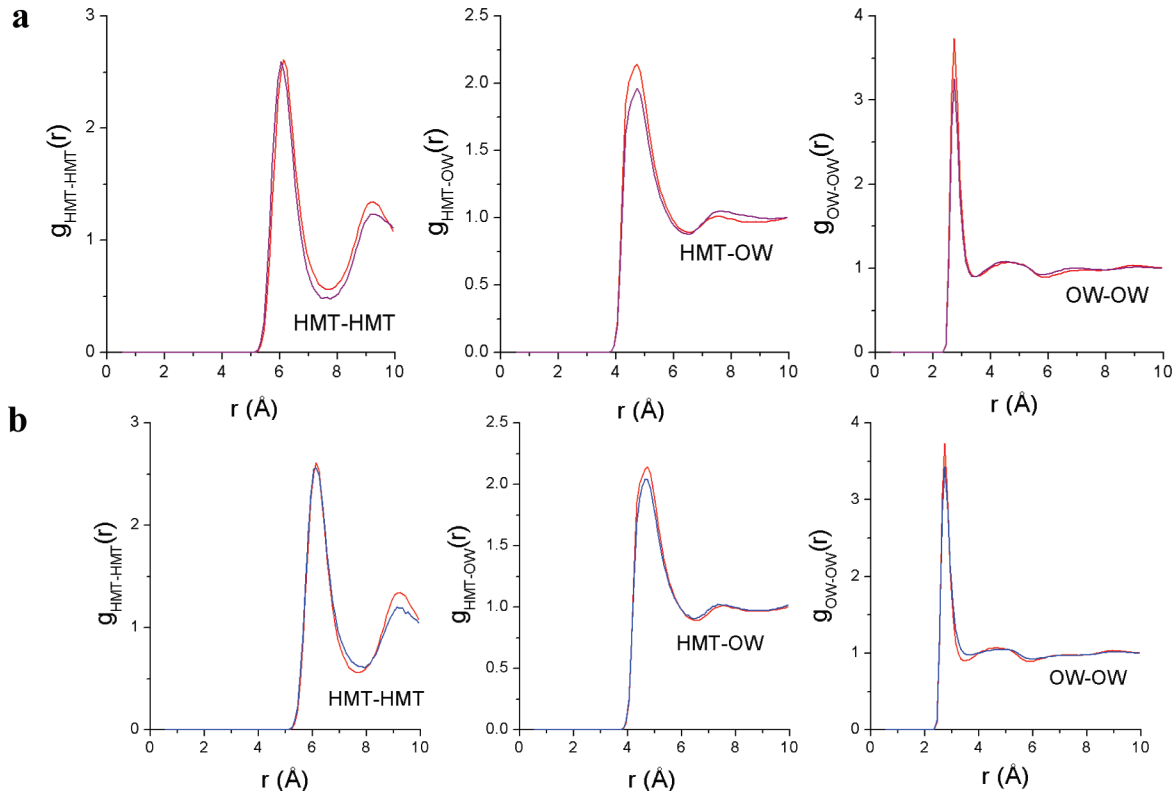

Figure 3. Molecular centers' functions (a) for 0.05 mol fraction of aqueous HMT (purple) compared to 0.095 mol fraction aqueous HMT (red) both at 25 °C; (b) for 0.095 mol fraction of aqueous HMT at 80 °C (blue) compared to at 25 °C (red). Center of HMT molecule is defined as the geometric center of the six carbon and four nitrogen atoms that make up HMT, and the center of the water molecule is the OW atom.

as the aforementioned geometrical and density constraints imposed by the simulation reduce the sensitivity of the structural interpretation to any residual systematic errors in the data.

Partial Distribution Functions

General Comments. Figure 2 also shows the seven composite radial distribution functions derived from the combination of experimental data and EPSR modeling. In examining the detailed structures of the solutions it is necessary to access selected partial radial distribution functions. There are 16 intermolecular site−site partial distribution functions (PDFs) for the HMT−water system arising from the distinguishable atomic sites on the HMT and water molecules. These partial distribution functions, $g_{\alpha\beta}(r)$, give the correlations between atoms of type α on one molecule and atoms of type β on other molecules. Intramolecular correlations are constrained by ESPR within reasonable molecular configurations and are effectively subtracted from the data so that the evolution of the model is driven by the intermolecular contributions. In gaining an overview of the solution structure, the most convenient partial distribution functions to consider are those relating the molecular centers: HMT···HMT, OW···OW (for water−water), and HMT···OW (for HMT−water). The center of the water molecule is the OW atom and that of the HMT molecule is indicated in Figure 1b (the red sphere, the geometric center of the positions of the six carbon and four nitrogen atoms). These PDFs are compared in Figure 3 to explore the impact of composition at 25 °C and temperature at a constant mol fraction of 0.095. In making these comparisons the different relative atomic densities of the indistinguishable atomic sites of the 0.05 and 0.095 mol fraction solutions at 25 °C mean that quantitative inferences must be drawn from the numerical values of the co-ordination numbers given in Table 4 rather than the visualized peak heights in Figure 3.

Overall the global changes presented here (these functions are spatially averaged over all directions from the center of an HMT molecule and therefore do not reveal details of specific interactions) are all as expected with increasing concentration. For HMT···HMT contacts, increasing concentration leads to an increase in the first sphere co-ordination number from 1.9 to 3.3. Associated with this is a small shift in the $g(r)$ maximum from 6.05 to 6.15 Å, presumably as a result of steric effects since at the higher concentration there are more HMT molecules to fit in: 1 HMT molecule to 19 waters at 0.050 and 1 HMT to 10 waters at 0.095 mol fraction. Hence, perhaps in the more concentrated solution there are not enough waters available to fully hydrate the HMT, and this may also contribute to the shift in the HMT···HMT $g(r)$ maximum. The second co-ordination sphere around HMT increases from 2.7 to 4.7 with increasing concentration, so that the total HMT co-ordination around a central HMT molecule (up to a distance of 10 Å) increases from 4.6 to 8.0 on going from 0.050 to 0.095 mol fraction. At the same time the number of HMT−water contacts out to about 6.50 Å decreases from approximately 29 to 25 with a small shoulder accounting for about four water molecules between 3.7 and 4.6 Å at each temperature. These may be hydrogen bonded to the central HMT molecule. Water−water contacts diminish with increased concentration, the water−water $g(r)$ being very similar to pure water, suggesting little disruption to the overall water structure. This is in complete contrast to the case of 0.2 and 0.3 mol fraction aqueous urea where the 4.5 Å water peak is totally absent, indicating that dissolution of urea requires disruption of the water structure[9,10] which occurs only with increasing temperature.

TABLE 4: Average Co-ordination Numbers Calculated from Integration of the Relevant Partial Distribution Functions Shown in Figures 3 and 4 for a 0.05 Mol Fraction of HMT Solution and a 0.095 Mol Fraction of HMT Solution Both at 25°C Using the Atomic Density and Limits Indicated in the Table

correlation	R_{min}, Å	R_{max}, Å	atomic density ρ, atom Å^{-3}	0.095 aqueous HMT, 25 °C co-ordination number (atoms)	atomic density ρ, atom Å^{-3}	0.05 aqueous HMT, 25 °C co-ordination number (atoms)
HMT−HMT	5.00	7.75	0.0021	3.3 ± 0.3	0.0013	1.9 ± 0.4
	7.75	10.00		4.7 ± 0.4		2.7 ± 0.4
	5.00	10.00		8.0 ± 0.5		4.6 ± 0.5
OW−OW	2.00	3.30	0.0203	3.4 ± 0.1	0.0252	3.8 ± 0.1
	3.30	5.00		7.7 ± 0.2		9.7 ± 0.2
HMT−OW	3.70	4.55	0.0203	4.1 ± 0.3	0.0252	4.5 ± 0.4
	4.55	6.50		20.5 ± 0.6		24.1 ± 0.9
	3.70	6.50		24.6 ± 0.6		28.6 ± 0.9
OW−HMT	3.70	4.55	0.0021	0.4 ± 0.03	0.0013	0.2 ± 0.02
	4.55	6.50		2.1 ± 0.1		1.2 ± 0.04
	3.70	6.50		2.5 ± 0.1		1.4 ± 0.1
N−N	3.00	4.90	0.0085	1.3 ± 0.1	0.0053	0.8 ± 0.1
	4.90	7.50		10.3 ± 0.3		6.1 ± 0.3
	7.50	9.40		15.0 ± 0.4		8.7 ± 0.4
N−H	2.00	3.30	0.0256	0.6 ± 0.04	0.0159	0.4 ± 0.1
	3.30	9.00		68.1 ± 0.6		40.3 ± 0.6
C−C	2.75	4.10	0.0128	0.8 ± 0.1	0.0080	0.5 ± 0.1
	4.10	7.10		13.0 ± 0.3		7.8 ± 0.3
N−HW	1.50	2.65	0.0407	0.7 ± 0.1	0.0505	0.7 ± 0.1
	2.65	5.20		19.3 ± 0.3		22.2 ± 0.4
N−OW	2.50	3.30	0.0203	0.7 ± 0.1	0.0252	0.7 ± 0.1
	3.30	5.65		13.3 ± 0.2		15.4 ± 0.4
C−OW	2.50	4.50	0.0203	5.2 ± 0.1	0.0252	5.9 ± 0.2
H−OW	1.75	3.30	0.0203	1.7 ± 0.1	0.0252	1.9 ± 0.1
	1.75	4.60		6.4 ± 0.1		7.3 ± 0.1
OW−HW	1.00	2.40	0.0407	1.5 ± 0.1	0.0505	1.6 ± 0.1

Partial Radial Distribution Functions. The other important partial radial distribution functions are displayed for consideration in Figure 4. As with the molecular centers' PDFs, the general shape of the individual partial radial distribution functions is the same as the concentration is altered; however, the effect of concentration change on the co-ordination numbers in the solutions is detailed in Table 4. These results confirm the increase in HMT−HMT co-ordination with increasing concentration with the near neighbors N···N, N···H, and C···C contacts all increasing. Evidence for specific HMT···HMT interactions is seen in the N···H $g(r)$ (a in figure 4) which has a shoulder between 2 and 3.3 Å corresponding to approximately 0.60 molecules. This is consistent with the existence of a weak N···H−C hydrogen bond also found in the crystal structure at a distance of around 2.9 Å and shown in Figure 1d.

The peaks at 1.95 Å and 2.9 Å (b and c in Figure 4) in the N−HW and N−OW partial radial distribution functions are consistent with water molecules being hydrogen bonded to the nitrogens of HMT. This is apparently independent of concentration (average N−HW coordination out to 2.65 Å is 0.7 at both concentrations) despite the global fall in water co-ordination with rise in HMT concentration. The H−OW $g(r)$ has a slight shoulder at about 2.65 Å (d in Figure 4) which might indicate additional weak C−H···OW interactions. This contact is increased from 1.7 to 1.9 (up to a distance of 3.3 Å) upon dilution, is consistent with the increase in the C···OW co-ordination from 5.2 to 5.9 upon dilution, and may suggest a cause for the increase in waters found around the HMT molecules.

It appears that the specific interactions in solution are dominated by the hydration of HMT rather than HMT−HMT interactions. The impact of HMT on water structure is seen in the OW···OW and OW···HW partial radial distribution functions at both concentrations which are compared to the $g_{OW\text{-}OW}(r)$ and the $g_{OW\text{-}HW}(r)$ for pure water[32] in Figure 5. Considering first the general impact of HMT on water structure it is evident that as far as the OW···OW contacts are concerned, the nearest neighbor distances are relatively unaffected at either concentration. In all cases the first peak in the $g(r)$ occurs at 2.75 Å. However, the position of the second peak moves significantly from 4.55 Å in pure water and dilute HMT, to 4.65 Å in the more concentrated solution. Since the OW···OW function reflects the hydrogen bonded network present in the solutions, this is indicative of a perturbation of water structure in its second co-ordination shell. The nature of this alteration is discussed further when examining the OW···OW spatial density function below. This perturbation of the water hydrogen bonded network is also seen in the OW···HW co-ordination number which falls from 2 in pure water to 1.6 and 1.5 in the 0.050 and 0.095 mol fraction solutions, respectively.

This lowering of the co-ordination numbers reflects the ability of the HMT molecules to accept hydrogen bonds but not to donate them to the water.

Spatial Density Functions. Spatial density functions (SDFs,[8,33]) are three-dimensional maps showing the regions of space around a central molecule most likely to be occupied by the molecular centers of the neighboring molecules. Figures 6a and 6b show the SDFs for HMT−HMT interactions with only the nitrogen and carbon atoms on the central HMT molecule represented for clarity. For both concentrations there are lobes above all the faces of the central HMT molecule, suggesting the prevalence of face to face interactions. At the higher concentration of HMT (Figure 6b) it appears that the lobes extend beyond the face centers, taking in the nitrogen atoms. Figure 1e, taken from the crystal structure (HMTAM07), uses a space filling representation of the molecules to indicate how such face on interactions (N···H−C distance of 2.892 Å) are involved in the crystal structure: it appears that a very similar phenomenon exists in solution, with an N···H distance of about 2.6 Å.

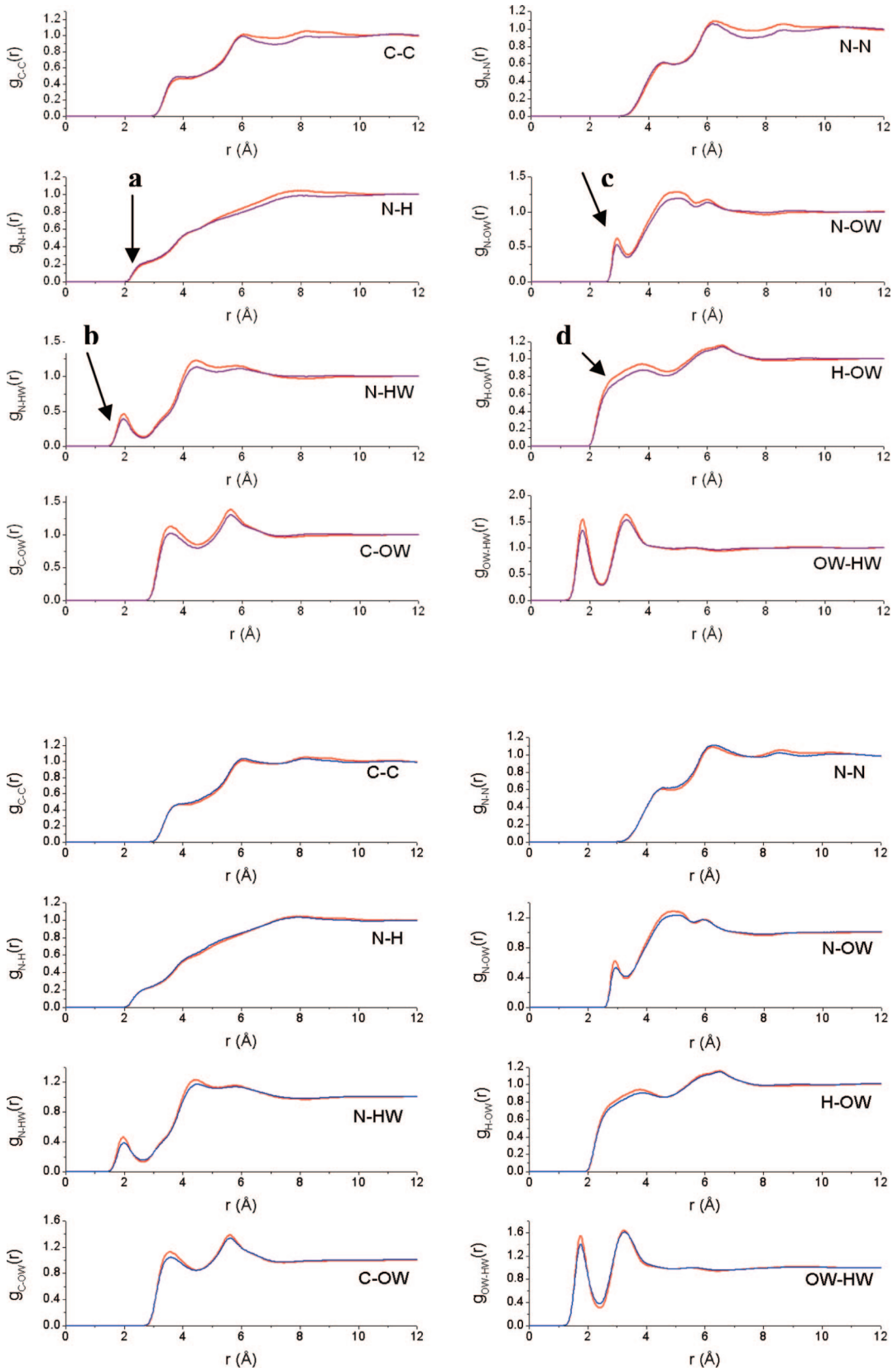

Figure 4. (top) Partial radial distribution functions for 0.05 mol fraction of aqueous HMT (purple) compared to 0.095 mol fraction aqueous HMT (red) both at 25 °C. (bottom) Partial radial distribution functions for 0.095 mol fraction of aqueous HMT at 80 °C (purple) compared to at 25 °C (red). Highlighted peaks, a, b, c, d are identified in the text.

Figures 6c and 6d, show the SDFs for water around HMT. These are significantly orientationally ordered with HMT effectively 'templating' the water within very well-defined spatial locations where it interacts with both the nitrogen atoms and the faces of the central HMT molecule. For HMT around water, the SDFs presented here in Figure 6e and 6f are slightly unusual with interactions occurring not only to the hydrogen atoms and the lone pairs of the water molecule but also normal

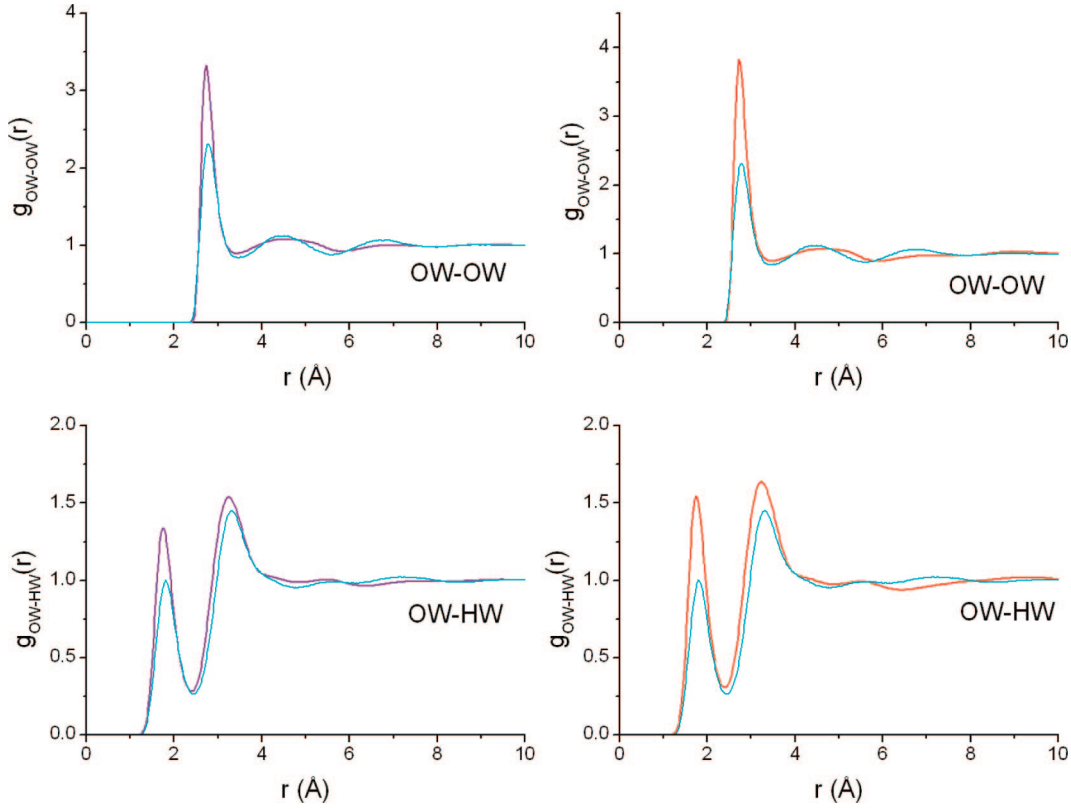

Figure 5. Water−water partial radial distribution function for aqueous HMT solutions at 25 °C compared to those for pure water at 25 °C (blue).[32] Left: 0.05 mol fraction of HMT aqueous solution (purple); right: 0.095 mol fraction of HMT aqueous solution (red).

to the HOH plane. This is consistent with the broad shape of the C−H···OW $g(r)$ (Figure 4).

Finally the water−water contacts are examined by looking at the SDFs generated for this interaction in Figure 7. Here it is seen that the OW···OW interactions in the first neighbor distance range 2.5−3.5 Å for both concentrations of HMT are similar to those for pure water, Figure 7c. This is expected from the similarity between the first peak of the relevant $g_{OW\text{-}OW}(r)$ functions for the pure water and for the solution seen in Figure 5. However, interactions in the distance range 3.5−5 Å differ from those in the pure water, particularly in the more concentrated solution. Here, the OW···OW SDF is not continuous; rather the orientations available to the second neighbor water molecules are more restricted. In the SDFs for both concentrations of HMT there is an extra lobe present directly underneath the oxygen atom which is not there for pure water. This indicates that the next most favorable positions of the water molecules appear to be closer in the HMT solutions than in pure water. Overall these data clearly show that the water structure is more spatially constrained in HMT solutions than in pure water, confirming at an atomistic level the earlier conclusions based on thermodynamic data.[19,20]

In the HMT hexahydrate, visualized in Figure 1f there are three water molecules hydrogen bonded to three nitrogen atoms of HMT at an N···OW distance of 2.817 Å with the remaining three water molecules forming interactions between the water oxygen and HMT hydrogens at distances of either 2.653 Å or 2.714 Å. It is now clear that these hydrogen bonded waters are also evident in solution in the 0.7 molecules in the N···OW co-ordination sphere at about 2.9 Å (Table 4 and Figure 4) while the H···OW interaction in the hydrate crystal is mirrored as a slight shoulder in the solution at 2.65 Å (Figure 4). Interestingly the orientation of the water in the hexahydrate is such as to give three water molecules directed to the HMT nitrogens and the other three positioned toward the HMT faces. This is also reflected in the SDFs shown in Figure 6 and overall suggests a strong link between the structuring in the solution and the appearance of a crystalline hexahydrate which hence requires only the removal of two waters from a central HMT molecule to achieve the appropriate coordination for the crystal.

Reviewing the two HMT aqueous solutions investigated, the data presented here provide a picture of the solution in which each HMT molecule is surrounded (at a distance up to 4.5 Å) by either 4.5 or 4.1 water molecules in the 0.050 or 0.095 mol fraction of aqueous HMT solutions, respectively (Table 4). Further out there are respectively 1.9 or 3.3 HMT molecules at a distance of 6.05 or 6.15 Å and an extra 24 or 20.5 water molecules at a distance of approximately 4.75 Å. The nitrogen on a central HMT molecule interacts with respectively 0.4 or 0.6 hydrogens on other HMT molecules and is hydrogen bonded to 0.7 water molecules at both concentrations. Around the water molecules there are 3.8 and 3.4 contacts with other water molecules in the 0.05 and 0.095 mol fraction aqueous HMT solutions respectively at a distance of 2.75 Å and 2.5 and 1.4 interactions to HMT at 4.75 Å. From the SDFs the HMT−HMT interactions are discovered to be face on, with the HMT−water and water−HMT contacts being a mix of hydrogen bonded and weak polar interactions. The presence of HMT in the 0.095 mol fraction aqueous solution disturbs the second co-ordination shell structure of the water, a perturbation which also exists, though to a lesser degree, at 0.050 mol fraction.

While it appears that the specific interactions in solution are dominated by the hydration of HMT, the HMT···HMT and HMT···water interactions show clear parallels between the solution structure and the crystal structure of both the anhydrous and hexahydrate forms. These similarities are evident from both the distances at which the specific interactions occur in the crystal structures and in solution and from the relative orientation

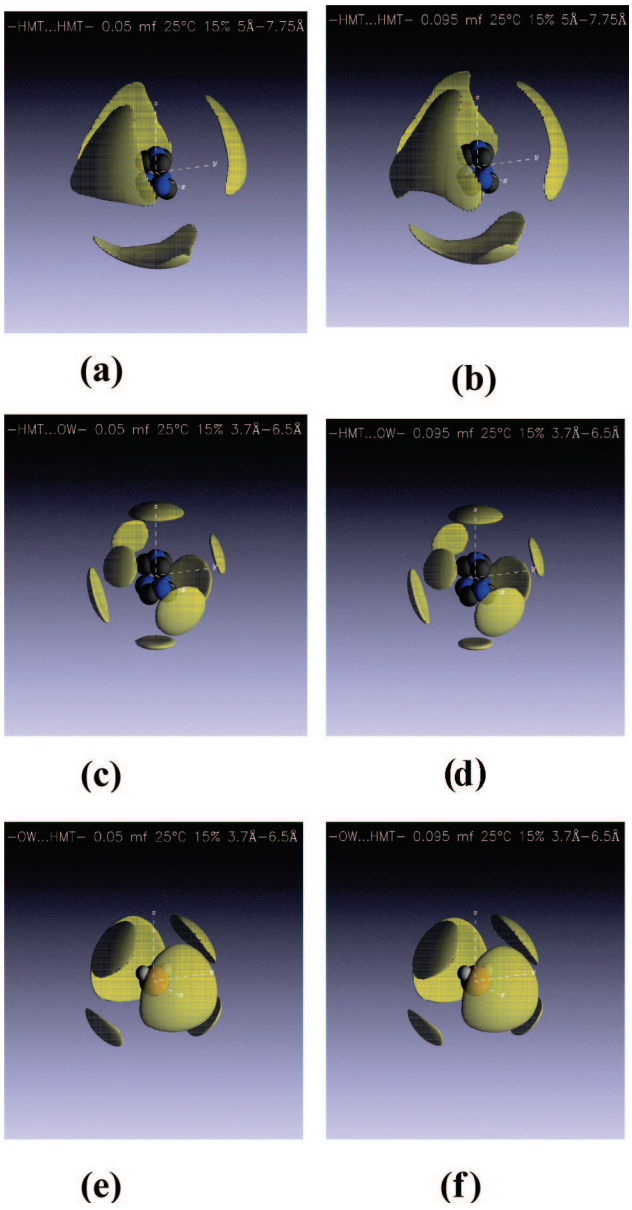

Figure 6. The spatial density functions derived for HMT around HMT, (a) 0.05 mol fraction aqueous HMT and (b) 0.095 mol fraction aqueous HMT; water around HMT, (c) 0.05 mol fraction aqueous HMT, and (d) 0.095 mol fraction aqueous HMT; HMT around water (e) 0.05 mol fraction aqueous HMT and (f) 0.095 mol fraction aqueous HMT, all at 25 °C. The viewports are centered on the geometric center of the positions of the carbon and nitrogen atoms on each HMT molecule and on Ow for water ± 10 Å with an isosurface level of 15% (in the distance range 5−7.75 Å for HMT−HMT and 3.7−6.5 Å for water−HMT and HMT−water).

of HMT and water revealed in the SDFs. From the perspective of the phase diagram and crystal nucleation this indicates a strong link between the solution structure and the temperature dependence of the two solid forms in the binary phase diagram (Figure 1c) and, as in our previous studies on urea and inosine,[4,9] indicates the pivotal importance of desolvation in the nucleation pathway. Thus, at temperatures below 13.5 °C the available thermal energy is only able to partially desolvate HMT molecules, removing one hydrogen bonded and one face bonded water and leading directly to the hexahydrate. However, with increasing temperature thermal effects weaken all the water···HMT interactions, allowing nucleation to proceed directly to the totally desolvated, anhydrous crystal form.

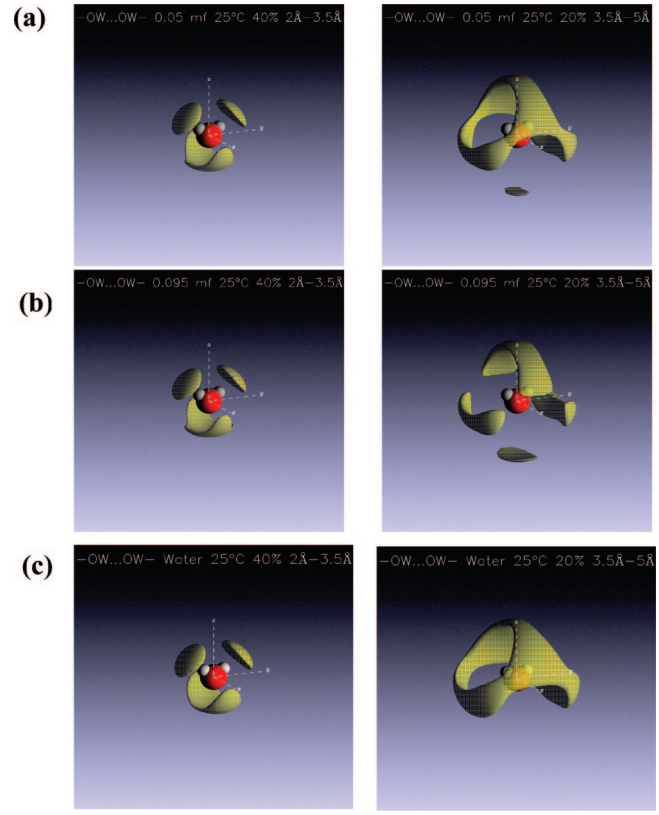

Figure 7. The spatial density functions derived for water around water (OW center of water) for (a) 0.05 mol fraction aqueous HMT both at 25 °C, (b) 0.095 mol fraction aqueous HMT, and (c) pure water[32] all at 25 °C. The viewports in each case are centered on the OW atom ± 10 Å with an isosurface level of (left) 40% (in the distance range 2.5−3.5 Å) and (right) 20% (in the distance range 3.5−5 Å).

The Effect of Temperature: Comparing 0.095 Mol Fraction Aqueous HMT at 25 and 80 °C. The molecular centers' and partial radial distribution functions of a 0.095 mol fraction HMT aqueous solution at 80 °C were compared to those for the same concentration at 25 °C. These are shown in Figures 3 and 4. Average co-ordination numbers are shown in Table 5. As with the solution at 25 °C, the HMT···HMT interactions occur at a distance of 6.15 Å at 80 °C. However, the HMT···HMT $g(r)$ shows a slight difference in the height of the first peak which, given the equality of the atomic densities between the two solutions, implies a difference in structure between the two temperatures. In particular the average number of first neighbor HMT···HMT contacts increases from 3.3 to 3.5 (see Table 5) on approaching the solubility minimum, an increase of 6% although the solubility change over this temperature range is only 3%. At a distance of 10 Å there are very slightly fewer HMT−HMT contacts at the higher temperature with the total co-ordination decreasing very slightly from 8.0 to 7.9. The HMT−water contacts are closer at the higher temperature with the HMT···OW interaction occurring at 4.65 Å compared to 4.75 Å at 25 °C. There are 3.7 water molecules in the distance range 3.7−4.55 Å (cf 4.1 at 25) and again the slight shoulder in the HMT···OW $g(r)$ could be due to hydrogen bonding although it is not as prevalent as in the solution at 25 °C. The total hydration of HMT is 23.2 (±0.6) water molecules in the distance range 3.7−6.5 Å at 80 °C, which is reduced compared to the 24.6 (±0.6) interactions occurring at 25 °C. This is consistent with the reduced solubility at 80 °C. Conversely, the HMT solvation of the water molecules indicated by the OW···HMT co-ordination numbers is constant with the

TABLE 5: Average Co-ordination Numbers Calculated from Integration of the Relevant Partial Distribution Functions Shown in Figures 3 and 4 for a 0.095 Mole Fraction of HMT Solution at 25°C and 80°C Using the Atomic Density and Limits Indicated in the Table

correlation	R_{min}, ÅA	R_{max}, ÅA	atomic density ρ, atom ÅA^{-3}	0.095 aqueous HMT, 25 °C Co-ordination number (atoms)	atomic density ρ, atom ÅA^{-3}	0.095 aqueous HMT, 80 °C Co-ordination number (atoms)
HMT−HMT	5.00	7.75	0.0021	3.3 ± 0.3	0.0021	3.5 ± 0.3
	7.75	10.00		4.7 ± 0.4		4.4 ± 0.4
	5.00	10.00		8.0 ± 0.5		7.9 ± 0.5
OW−OW	2.00	3.30	0.0203	3.4 ± 0.1	0.0197	3.4 ± 0.1
	3.30	5.00		7.7 ± 0.2		7.5 ± 0.2
HMT−OW	3.70	4.55	0.0203	4.1 ± 0.3	0.0197	3.7 ± 0.2
	4.55	6.50		20.5 ± 0.6		19.4 ± 0.6
	3.70	6.50		24.6 ± 0.6		23.2 ± 0.6
OW-HMT	3.70	4.55	0.0021	0.4 ± 0.03	0.0021	0.4 ± 0.03
	4.55	6.50		2.1 ± 0.1		2.1 ± 0.1
	3.70	6.50		2.5 ± 0.1		2.4 ± 0.1
N−N	3.00	4.80	0.0085	1.1 ± 0.1	0.0085	1.2 ± 0.1
	4.90	7.50		10.5 ± 0.3		10.7 ± 0.3
	7.50	9.40		15.0 ± 0.4		14.3 ± 0.4
N−H	2.00	3.30	0.0256	0.6 ± 0.04	0.0248	0.6 ± 0.1
	3.30	9.00		68.1 ± 0.6		66.0 ± 0.5
C−C	2.75	4.00	0.0128	0.6 ± 0.1	0.0128	0.7 ± 0.1
	4.00	7.10		13.1 ± 0.3		13.4 ± 0.3
	7.10	9.90		33.9 ± 0.4		32.2 ± 0.4
N−HW	1.50	2.65	0.0407	0.7 ± 0.1	0.0394	0.6 ± 0.1
	2.65	5.20		19.3 ± 0.3		18.0 ± 0.3
	5.20	8.25		75.0 ± 0.6		72.8 ± 0.6
N−OW	2.50	3.30	0.0203	0.7 ± 0.1	0.0197	0.6 ± 0.1
	3.30	5.65		13.3 ± 0.2		12.6 ± 0.2
	5.65	8.00		28.9 ± 0.4		28.2 ± 0.4
C−OW	2.50	4.50	0.0203	5.2 ± 0.1	0.0197	4.8 ± 0.1
	4.50	7.50		30.6 ± 0.3		29.6 ± 0.3
H−OW	1.75	3.30	0.0203	1.7 ± 0.1	0.0197	1.5 ± 0.1
	1.75	4.60		6.4 ± 0.1		6.0 ± 0.1

temperature increase at 2.5 molecules in the distance range 3.7−6.5 Å. The water−water contacts revealed in the OW···OW $g(r)$ (Figure 3) also remain unchanged with increase in temperature. There are 3.4 water molecules around a central water molecule in the distance range 2−3.3 Å (Table 5) and a further 7.5 water molecules in the distance range 3.3−5 Å, which is slightly less than in the solution at 25 °C.

The nature of the increased segregation of the HMT molecules, as indicated by the increased HMT···HMT co-ordination, was investigated further by examining the remaining HMT···HMT partial radial distribution functions where the increased C···C-and N···N- co-ordination support this overall picture (Table 5). Such behavior must be accompanied by changes in the HMT−water contacts, and these are seen from Table 5 as decreases in the N···OW-, N···HW, and C···OW functions at 80 °C compared to 25 °C.

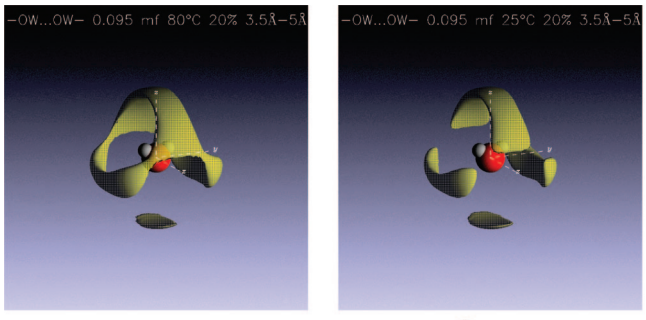

Figure 8. The spatial density functions derived for water around water (OW center of water) for a 0.095 mol fraction of aqueous HMT solution (a) at 80 °C and (b) at 25 °C. The viewports in each case are centered on the OW atom ± 10 Å with an isosurface level of 20% (in the distance range 3.5−5 Å).

The SDFs generated to accompany the molecular center radial distribution functions for the solution at 80 °C have an almost identical form to those at 25 °C and so have not been shown.

However, there are very subtle differences which will be discussed here. At 80 °C the HMT···HMT SDF indicates that this first neighbor interaction is more restricted than that for 25 °C while the HMT···OW and OW···HMT SDFs show slightly more disorder. This is consistent with increased HMT−HMT contacts and decreased HMT−OW contacts at 80 °C. The SDFs for the OW···OW interaction (Figure 8) are the same for the first co-ordination shell of water but are different for the second co-ordination shell. Here it is evident that as the temperature is increased, the water environment becomes restored closer to that in pure water (Figure 7c). Overall, in agreement with the conclusions from thermodynamic reasoning,[21] these data suggest that the more ordered the water environment the more soluble the HMT, since at 25 °C the second water shell is more orientationally restricted and HMT more soluble than at 80 °C.

Conclusions

The data presented here provide a picture of the solution in which each HMT molecule is surrounded (at a distance up to 4.5 Å) by approximately four water molecules in the three solutions investigated. Further out there are either just under two or just over three HMT molecules at a distance of 6.05 or 6.15 Å and an extra 24 or 20 water molecules at a distance of approximately 4.75 Å in the 0.050 or 0.095 mol fraction aqueous HMT solution at 25 and 80 °C, respectively. Clear similarities exist between solution structure and the crystalline hexahydrate; these similarities are reduced with increasing temperature as

the average number of water molecules hydrogen bonded to each nitrogen on a central HMT molecule is reduced fractionally from 0.7 to 0.6. From the SDFs the HMT···HMT interactions are discovered to be face on, involving weak C−H···N interaction while the HMT−water and water−HMT contacts are a mix of hydrogen bonded and weak polar interactions. The HMT−water SDF shows how an HMT molecule can template the solvent. Overall, the presence of HMT in the 0.095 mol fraction of HMT aqueous solution disturbs the second co-ordination shell structure of the water in the solution, an effect which is present to a lesser degree in the 0.050 mol fraction solution. At 80 °C the HMT molecules are more segregated and the HMT−water interactions are decreased compared to the contacts occurring at 25 °C. This is consistent with the lower solubility in the higher temperature system. Although the water co-ordination remains constant with temperature, the occupancy of surrounding water shells becomes more orientationally continuous when the temperature is increased, suggesting that the more orientationally ordered the water environment the more soluble the HMT. This conclusion finds similarities with the previous studies of Barone et al.,[21] Quadrifoglio et al.,[20] and Crescenzi et al.[19] who all found evidence from physicochemical properties and thermodynamic data of aqueous HMT solutions to suggest that HMT acts to enhance water structure. The current work presented here begins to clarify, and quantify, the nature of this structural enhancement.

Supporting Information Available: Experimental details. This material is available free of charge via the Internet at http://pubs.acs.org.

References and Notes

(1) Prausnitz, J. M.; Lichtenthaler, R. N.; de Azevedo, E. G. *Molecular thermodynamics of fluid-phase equilibria*, 3rd ed.; Prentice Hall Inc.: Upper Saddle River, NJ, 1998.

(2) Spitaleri, A.; Hunter, C. A.; McCabe, J. F.; Packer, M. J.; Cockroft, C. S. L. *Cryst. Eng. Commun.* **2004**, *6*, 489–493.

(3) Davey, R. J.; Mughal, R. G.; Parveen, S. *Cryst. Growth Des.* **2006**, *6*, 1788–1796.

(4) Chiarella, R. A.; Gillon, A. M.; Burton, R. C.; Davey, R. J.; Sadiq, G.; Auffret, A.; Cioffi, M.; Hunter, C. A. *Faraday Discuss.* **2007**, *136*, 179–193.

(5) Soper, A. K. *Chem. Phys.* **1996**, *202*, 295–306.

(6) Soper, A. K. *Mol. Phys.* **2001**, *99*, 1503–1516.

(7) Dixit, S.; Crain, J.; Poon, W. C. K.; Finney, J. L.; Soper, A. K. *Nature (London)* **2002**, *416*, 829–832.

(8) Bowron, D. T.; Finney, J. L.; Soper, A. K. *J. Phys. Chem. B* **1998**, *102*, 3551–3563.

(9) Soper, A. K.; Castner, E. W.; Luzar, A. *Biophys. Chem.* **2003**, *105*, 649–666.

(10) Burton, R. C.; Ferrari, E.S.; Davey, R. J.; Hopwood, J.; Quayle, M. J.; Finney, J. L.; Bowron, D. T. *Cryst. Growth Des.* **2008**, 1559–1565.

(11) White, E. T. *J. Chem. Eng. Data* **1967**, *12*, 285–289.

(12) Dickinson, R. G.; Raymond, A. L. *J. Am. Chem. Soc.* **1923**, *45*, 22–29.

(13) Terpstra, M.; Craven, B. M.; Stewart, R. F. *Acta Crystallogr. A* **1993**, *49*, 685–692.

(14) Mak, T. C. W. *J. Chem. Phys.* **1965**, *43*, 2799–2805.

(15) Walker, J. F. *Formaldehyde*; Reinhold Publishing Corp.: New York, 1964.

(16) Davey, R. J.; Rutti, A. *J. Cryst. Growth* **1976**, *32*, 221–226.

(17) Denbigh, K. G.; White, E. T. *Chem. Eng. Sci.* **1966**, *21*, 739–754.

(18) Jeffrey, G. A.; Mak, T. C. W. *Science* **1965**, *149*, 178–179.

(19) Crescenzi, V.; Quadrifoglio, F.; Vitaglia, V. *J. Phys. Chem.* **1967**, *71*, 2313–2318.

(20) Quadrifoglio, F.; Crescenzi, V.; Cesaro, A.; Delben, F. *J. Phys. Chem.* **1971**, *75*, 3633–3635.

(21) Barone, G.; Crescenz, V.; Liquori, A. M.; Quadrifoglio, F. *J. Phys. Chem.* **1967**, *71*, 984–986.

(22) Finney, J. L.; Soper, A. K. *Chem. Soc. Rev.* **1994**, *23*, 1–10.

(23) Bowron, D. T.; Finney, J. L.; Soper, A. K. *J. Am. Chem. Soc.* **2006**, *128*, 5119–5126.

(24) Soper, A. K. *Phys. Rev. B* **2005**, *72*, 104204−1104204−12.

(25) Berendsen, H. J. C.; Grigera, J. R.; Straatsma, T. P. *J. Phys. Chem.* **1987**, *91*, 6269–6271.

(26) Soper, A. K. *Chem. Phys.* **2000**, *258*, 121–137.

(27) Rizzo, R. C.; Jorgensen, W. L. *J. Am. Chem. Soc.* **1999**, *121*, 4827–4836.

(28) Wick, C. D.; Stubbs, J. M.; Rai, N.; Siepmann, J. I. *J. Phys. Chem. B* **2005**, *109*, 18974–18982.

(29) Soper, A. K.; Luzar, A. *J. Chem. Phys.* **1992**, *97*, 1320–1331.

(30) Bowron, D. T.; Moreno, S. D. *J. Chem. Phys.* **2002**, *117*, 3753–3762.

(31) Dixit, S.; Soper, A. K.; Finney, J. L.; Crain, J. *Europhys. Lett.* **2002**, *59*, 377–383.

(32) Soper, A. K. J. *Phys. Condens. Matter* **2007**, *19*, 335206–335224.

(33) Bowron, D. T.; Finney, J. L.; Soper, A. K. *Mol. Phys.* **1998**, *93*, 531–543.

JP811515U